PERGAMON

Aerosol Science 32 (2001) 489–508

Journal of
Aerosol Science

www.elsevier.com/locate/jaerosci

Numerical characterization of the morphology of aggregated particles

A. M. Brasil[a], T. L. Farias[a,*], M. G. Carvalho[a], U. O. Koylu[b]

[a]*Departamento de Engenharia Mecânica, Instituto Superior Técnico, Universidade Técnica de Lisboa, Av. Rovisco Pais, 1049-001 Lisbon, Portugal*

[b]*Department of Mechanical Engineering, Florida International University, Miami, FL 33174, USA*

Received 30 January 2000; received in revised form 21 July 2000; accepted 7 August 2000

Abstract

The structures of both cluster–cluster and particle–cluster fractal-like aggregates were investigated in the present study. Statistically significant populations of numerically simulated aggregates having appropriate fractal properties and prescribed number of primary particles per aggregate were generated in order to characterize three-dimensional morphological properties of aggregates, such as fractal dimension, fractal pre-factor, coordination number distribution function, and distribution of angles between triplets. Effects of aggregation mechanisms (i.e., cluster–cluster or particle–cluster) and aggregate size were taken into consideration. In addition, the morphological properties of aggregates undergoing partial sintering and restructuring were also investigated. To fulfill these objectives, aggregates were initially built without considering sintering or restructuring effects. Partial sintering of primary particles was then considered by introducing a penetration coefficient that allows touching particles to approach each other. Restructuring of aggregates was modeled during the process of building the cluster–cluster aggregates. For each pair of clusters that were attached together due to the normal aggregation procedure, a further mechanism was included that allowed the cluster to collapse until a more compact and stable position was achieved. The population studied was composed of ca. 450 simulated aggregates having a number of primary particles per aggregate between 8 and 1024. Calculations were performed for aggregates having a penetration coefficient in the range of 0–0.25 with and without restructuring. The following properties were investigated: fractal dimension, fractal pre-factor, coordination number distribution function, angle between triplets, and aggregate radius of gyration.

Keywords: Aggregate morphology; Clusters; Fractal-like aggregates; Triplets; Sintering

* Corresponding author. Tel.: + 351-21-841-7929; fax: + 351-21-847-5545.
E-mail address: fariastl@navier.ist.utl.pt (T. L. Farias).

0021-8502/01/$ - see front matter
PII: S0021-8502(00)00097-5

Nomenclature

a	primary particle radius
C_p	overlap coefficient
d_{ij}	distance between two particles
d_p	primary particle diameter
D_f	aggregate fractal dimension
k_g	fractal pre-factor (see Eq. (1))
N	number of primary particles in an aggregate
R_g	radius of gyration of an aggregate
$R_{g,r}$	radius of gyration of an aggregate with restructuring
Z	coordination number of particles

Greek letters

θ	angle between triplets

1. Introduction

Several types of solid pollutants (such as soot or inorganic materials) are frequently comprised of small monomers (primary particles) that coagulate to form large aggregates with fairly complex morphologies. Fortunately, these aggregates exhibit fractal-like properties which simplify their morphological characterization. This has been demonstrated experimentally and supported by numerical studies by several investigators (see Koylu, Xing, & Rosner, 1995b) and references cited therein). In particular, for fractal-like aggregates, the number of primary particles in an aggregate, N, scales with the radius of gyration, R_g, as follows:

$$N = k_g(R_g/a)^{D_f}. \tag{1}$$

Here, k_g is the fractal pre-factor (also known as the structural coefficient) and D_f the fractal dimension. Unfortunately, the knowledge of these variables is difficult; thus, most investigators have been forced to estimate the fractal dimension by light scattering or studied projected images of collections of aggregates in order to better understand their morphology and estimate both N and R_g (see Samson, Mulholand, & Gentry, 1987; Megaridis & Dobbins, 1990; Koylu et al., 1995b; Cai, Lu, & Sorensen, 1995). The majority of these studies involved analysis of transmission electron microscope (TEM) projected images of aggregates and required simple relationships between the two-dimensional visible information and the real three-dimensional properties of aggregates. Nelson, Crookes, and Simons (1990) and Koylu, Faeth, Farias, and Carvalho, (1995b) have reported important information in that field but limited their studies to the particular case of soot aggregates without taking into consideration important properties such as aggregate total surface and overlapping of primary particles. Oh and Sorensen (1997) investigated the latter subject, in particular the effect of partial overlapping on the expressions used to infer three-dimensional properties from projected images. More recently, Brasil, Farias, and Carvalho (1999a) have unified

most of those ideas and presented a recipe where, based on the projected images of fractal-like aggregates, all relevant morphological properties can be inferred. These findings are very encouraging especially for aggregates that do not suffer any severe restructuring while being generated or transported. Unfortunately there are particular applications, for example in the production of inorganic nanosize particles, where partial sintering and/or restructuring may occur due to high temperatures. Therefore, the resulting aggregate can be quite different in terms of the morphology and fractal dimension. In addition, past studies in this field have not addressed important properties such as the coordination number distribution function, or the distribution of angles between three touching particles (triplets or trimers). These properties are important in several applications, such as estimating the effective thermal conductivity or fabric tensor of an aggregate and characterizing aggregate structural stability (Tassopoulos & Rosner, 1992).

Based on these observations, the present investigation seeks to contribute to a better understanding of the morphology of fractal-like aggregates. In order to achieve this objective, the structures of both cluster–cluster (C–C) and particle–cluster (P–C) fractal-like aggregates were investigated. Statistically significant populations of numerically simulated aggregates having appropriate fractal properties and prescribed numbers of primary particles per aggregate were generated in order to characterize three-dimensional morphological properties of aggregates, namely the fractal dimension, D_f, structural coefficient, k_g, coordination number distribution function, Z, distribution of angles between triplets, θ, and aggregate radius of gyration, R_g. Moreover, effects of aggregation mechanisms (i.e., C–C or P–P) and aggregate size were taken into consideration.

The paper begins with a description of the numerical simulation procedure adopted to generate the fractal-like aggregates. The population of aggregates used for the present investigation is then fully characterized; in particular, the fractal dimensions and aggregate sizes are defined. The paper follows with an investigation of the fractal and morphological properties of C–C as well as P–C aggregates. The second part of the present work investigates the effects of partial sintering and aggregate restructuring on the morphological and fractal properties of C–C aggregates. Finally, the major conclusions are summarized.

2. Numerical simulation procedures

2.1. Simulation of aggregates

Various procedures to construct agglomerates composed of spherical primary units have been discussed by Jullien and Botet (1987), and Botet and Jullien (1988). These methods are based on simple algorithms that mimic C–C or P–C aggregation processes due to the Brownian motion. Several investigators (e.g. Vold, 1963; Hutchinson & Sutherland, 1965; Witten & Sander, 1981, 1983; Meakin, 1983a, b) have adopted P–C methods because of their simplicity. A more physically based method was developed by Mountain and Mulholland (1988) who generated soot aggregates using a numerical simulation involving C–C aggregation. Based on the solution of the Langevin equations, this approach yields fractal-like aggregates that satisfy the power-law relationship of Eq. (1) with D_f ca. 1.9 and k_g roughly 1.5 for $N > 10$. However, a larger sample of aggregates was needed for the present study, and it was also required that the present aggregates have specific

fractal dimensions and penetration coefficients. As a result, an alternative simulation method previously used by Farias, Carvalho, and Koylu, (1995, 1996), Koylu et al. (1995a) and Brasil et al. (1999a) was applied during the present investigation.

The aggregate simulation method creates a population of aggregates by C–C aggregation using a sequential algorithm that satisfies Eq. (1) intrinsically, rather than performing numerical simulations based on the Langevin dynamics, similar to the approach used by Mountain and Mulholland (1988). For pre-specified values of D_f and k_g, the aggregate generation process was initiated by randomly attaching individual and pairs of particles to each other. The attachment procedure was comprised of randomly choosing points of contact at the surface of two randomly chosen particles from two clusters (or pair at the beginning of the process). Uniform distributions of the point and orientation of attachment were assumed, while rejecting configurations where primary particles intersected. Further, because control of the fractal properties (D_f and k_g) was desired, the radius of gyration of the new aggregate was calculated based on the known positions of the primary particles, and checked to see if Eq. (1) was satisfied for the fractal dimension and pre-factor selected. If Eq. (1) was not satisfied, the cluster was discarded. This procedure was continued in order to form progressively larger aggregates that obeyed the statistical relationships of mass fractal objects. As a default, a hierarchical approach was used where only clusters having the same number of primary particles (or a similar number if N was odd) were joined together (Jullien & Botet, 1987). Nevertheless, if desired, the model was capable of creating non-hierarchical aggregates.

As previously discussed, the present algorithm can be applied to all types of fractal-like aggregates ($1 < D_f < 3$). By forcing the fractal dimension to fall between two pre-defined limits, in principle, these objectives could be created conveniently. Nevertheless, in practice, if a C–C procedure is adopted, the probability of constructing aggregates with large fractal dimension (say $D_f > 2.2$) rapidly approaches zero as the aggregate size, N, increases. This is understandable because the compactness required for aggregates with $D_f \to 3.0$ is not feasible using a C–C simulation approach that naturally leads to open-structured morphologies. For these situations a P–C mechanisms has to be adopted. The simulation procedure is similar to the C–C algorithm but individual particles, instead of clusters of spherical units, were attached to the main aggregate. This approach allows the user to construct aggregates having a wider range of fractal dimensions. Nevertheless, care must be taken when constructing aggregates having lower values of D_f because although Eq. (1) is still numerically satisfied, the aggregates lose their fractal properties (Jullien and Botet, 1987). Thus, the P–C algorithm is particularly appropriate to create compact clusters having larger fractal dimensions. These considerations will be addressed in more detail later on, while characterizing the fractal properties of the population of aggregates. Projected images of simulated C–C and P–C aggregates having different number of primary particles are illustrated in Fig. 1.

2.2. Simulation of sintering

Most numerical models that simulate agglomerates of spherical particles assume that neighboring monomers touch on a single point. Real aggregates do not satisfy this ideal condition. In fact, there are several different physical and environmental effects that contribute to a certain degree of penetration (or overlap) leading to more compact and rigid aggregates. Namely, there could be strong attraction forces between particles and/or lack of rigidity of the particle matter when aggregates cross high-temperature environments or due to the impact between the monomers

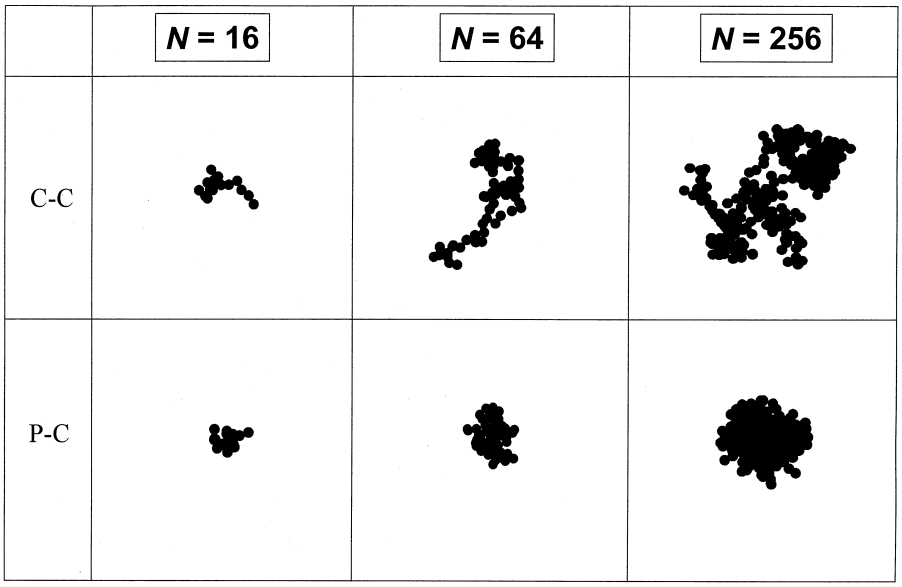

Fig. 1. Projected images of typical simulated cluster–cluster and particle–cluster aggregates.

when attaching to each other. In the present paper, the term sintering will be related to this partial overlapping of primary particles, which unavoidably exists between two (or more) touching particles in real aggregates. Consequently, a penetration coefficient, C_p, was defined as follows:

$$C_p = (d_p - d_{ij})/(d_p). \tag{2}$$

Here, d_{ij} represents the distance between two touching particles and d_p the diameter of uniform-size primary particles. If $C_p = 0$ the primary particles are in point contact whereas $C_p = 1$ indicates total sintering, i.e., every couple of neighbors merged into a single particle. Numerically, overlapping was accounted for by progressively increasing the diameters of the primary particles within an aggregate while maintaining the position of the center of the particle, followed by a scaling correction to keep the same reference value for particle diameter. Fig. 2 shows projected images of typical C–C aggregates having $N = 16$ and 64, and $C_p = 0$, 0.15 and 0.25 constructed using the aforementioned simulation procedure.

2.3. Simulation of restructuring

In many practical situations, aggregates may undergo a restructuring process where their open branched structure collapses, resulting in a more compact cluster. This can occur, for example, when the bond between the touching particles is weak or when harsh environments are encountered. In general, restructuring may be considered as another mechanism that can cause aggregate structure to become more compact.

In order to model the restructuring process during the present study, after two clusters coagulate and the fractal dimension of the resulting aggregate is checked, the following steps are introduced

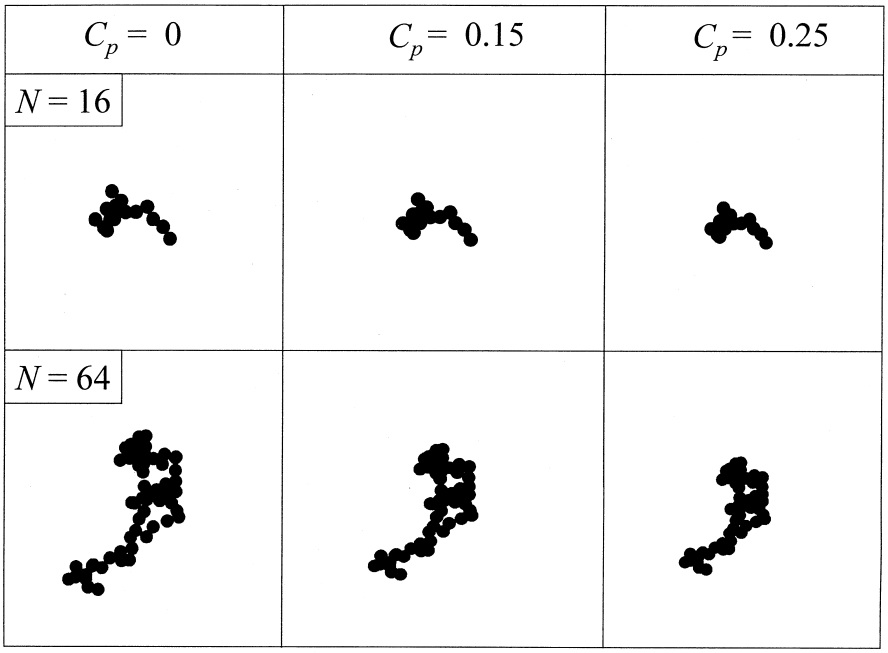

Fig. 2. Projections of typical simulated aggregates with partial sintering.

in the algorithm:

(i) two clusters that form a new aggregate will approach each other using the touching point as the center of rotation;
(ii) rotation will occur approaching the two centers of mass in the same plane, as if the two clusters would attract each other by the center of mass;
(iii) collapse of the two clusters will terminate when the number of contact points between the clusters is increased by one.

Restructuring will be introduced in all actions that involve the aggregation of two clusters (i.e., along the procedure of the simulation of the aggregate until N is reached). Fig. 3 shows the typical differences between the histogram of the same aggregate constructed with and without restructuring.

2.4. Population of fractal-like aggregates

In the present study, a well-defined population of fractal-like aggregates was desired. Therefore, the first issue was to select the most appropriate fractal dimensions. Although the fractal dimension has received considerable attention in the past, the selection of universal values for the fractal pre-factor for C–C aggregates is still a controversial issue. Wu and Friedlander (1993) and, more recently, Koylu et al. (1995b) have unified most of the numerical and experimental data reported on this property. For example, for C–C aggregates, experimental results published in the literature for k_g indicate values between 1.23 (Cai et al., 1995) and 3.47 (Samson et al., 1987). The range of results published varies by more than 200%, clearly showing that this issue deserves more attention.

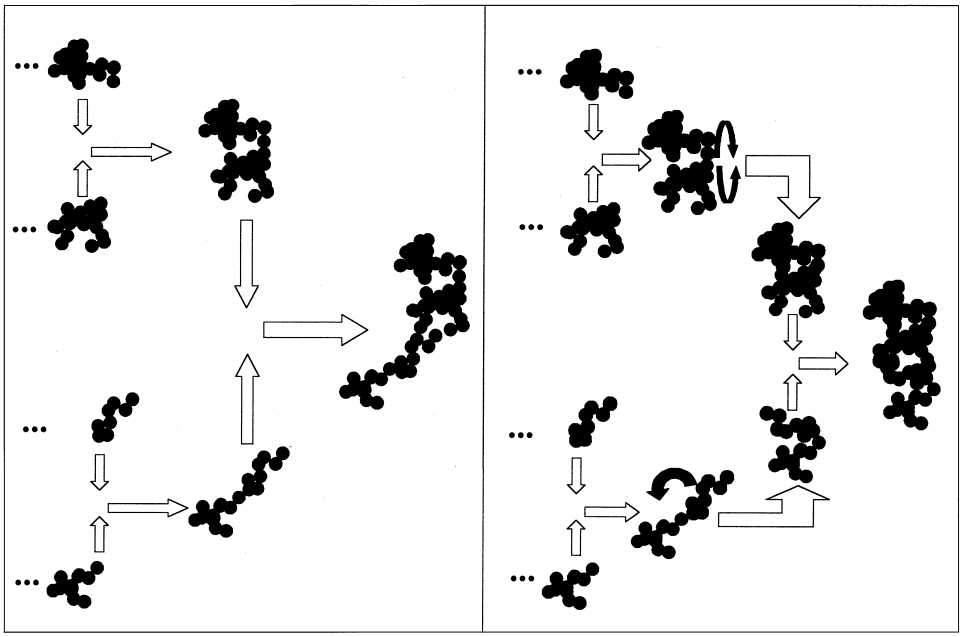

Fig. 3. Formation process of cluster–cluster aggregates: (a) where restructuring is not considered; and (b) undergoing restructuring.

In spite of the range of values published, it was noted that results based on numerically simulated aggregates were always about a factor of two lower than those inferred from experimental data (please see, Samson et al., 1987; Megaridis & Dobbins, 1990; Wu & Friedlander, 1993; Cai et al., 1995; Koylu et al., 1995a, b; Sorensen & Feke, 1996; Sorensen & Roberts, 1997). Oh and Sorensen (1997) have investigated the effect of overlap between primary particles on the fractal properties and concluded that the fractal dimension and particularly the fractal pre-factor could vary considerably with the rate of overlapping. However, no final conclusion regarding the discrepancies between experimental results and numerical finding was achieved. Brasil et al. (1999) verified that the large discrepancies between the values reported for the fractal pre-factor appear to be related to the partial overlapping of primary particles that leads to an increase in k_g while keeping the fractal dimension approximately constant. Consequently, it can be concluded that aggregates without overlap should be simulated having lower values of fractal pre-factor, while as overlapping increases, k_g will also increase as systematically observed by several researchers.

More recently, Brasil, Farias, and Carvalho (2000) combined numerical predictions of light scattering with morphological fractal concepts based on Eq. (1) to estimate the fractal dimensions of C–C simulated aggregates. Their best estimates were $k_g = 1.27$ and $D_f = 1.82$ for aggregates with non-overlapping particles. Surprisingly, if no restrictions are imposed on the fractal properties of our simulated aggregates, we obtain $k_g = 1.45$ and $D_f = 1.88$. These results are in very good agreement with the great majority of the values presented by other authors for simulated

aggregates (see Wu & Friedlander, 1993 and references cited therein). Based on these considerations, aggregates with no spherule overlapping used throughout this work were simulated in such a manner to have k_g ca. 1.27 and D_f ca. 1.82. As will be discussed in detail later on, this choice allows us to be consistent with the experimental data, as the partial sintering of particles will cause an increase in k_g without a change in D_f.

The population of C–C as well as P–C aggregates involved N in the range 8–1024, considering 8 different aggregate sizes. Results obtained for each aggregate size class were averaged over 32 different aggregates to yield a total sample of ca. 450 aggregates. This sample size was established in order to obtain a numerical uncertainty (95% confidence) of less than 10% for the different variables investigated in the present study. A mean primary particle diameter of unity was used for the simulations. However, present results were normalized by d_p such that results became independent of spherule size. Finally, in order to simplify the amount of data plotted in most of the figures, only mean values are shown for each aggregate size.

3. Results and discussion

3.1. Fractal and morphological properties of C–C and P–C aggregates

3.1.1. Fractal properties

As discussed earlier, the simulated aggregates are mass-fractal like and statistically satisfy Eq. (1). This behavior is illustrated in Fig. 4, which includes both C–C and P–C aggregate populations used throughout the present investigation. The results presented in Fig. 4 are for just-touching particles (aggregates neither sintered nor restructured). The least-squares fit of these simulations yielded $D_f = 1.82$ and $k_g = 1.27$ for the set of C–C aggregates, while for the more compact P–C aggregates the log–log plot indicates $D_f = 2.75$ and $k_g = 0.51$. The pre-factor values for P–C aggregates reported in the literature (see Wu & Friedlander, 1993) agree with the results presented in Fig. 4. However, the fractal dimension of P–C aggregates is not well established. P–C on a lattice was the first approach to be implemented in computer simulations (Eden, 1961) with the Witten and Sander model (Witten & Sander, 1981), known as diffusion-limited aggregation (DLA), being the most important P–C model. Using this milestone model, Meakin, (1983a, b) reported D_f ca. 2.5 and showed that the resulting fractal dimension increases with less sticking probabilities of particles. Later on, Meakin (1984) generalized the values of fractal dimensions to 2.75–3.0 for the case of pure ballistic P–C model (developed by Vold, 1963; Sutherland, 1967). For the same case, Gouyet (1996) found fractal dimension to be 2.8, noting that the true value could probably be close to 3. Sorensen and Roberts (1997) also reported that $D_f = 2.5$ and $k_g = 0.68$–0.80 for DLA aggregates.

At this point, we would like to emphasize a fundamental difference between the C–C and P–C aggregates. Jullien and Botet (1987) argued that aggregates obtained from P–C methods may not be considered as true fractals, questioning the applicability of fractal concepts to this class of aggregates. Oh and Sorensen (1998) showed that P–C aggregates are not scale invariant and actually have C–C structure over short length scales. Apart from this controversy, numerically simulated aggregates with fractal dimensions above 2.5 are only possible to achieve using the P–C method. Moreover, aggregates with high fractal dimension exist in several applications

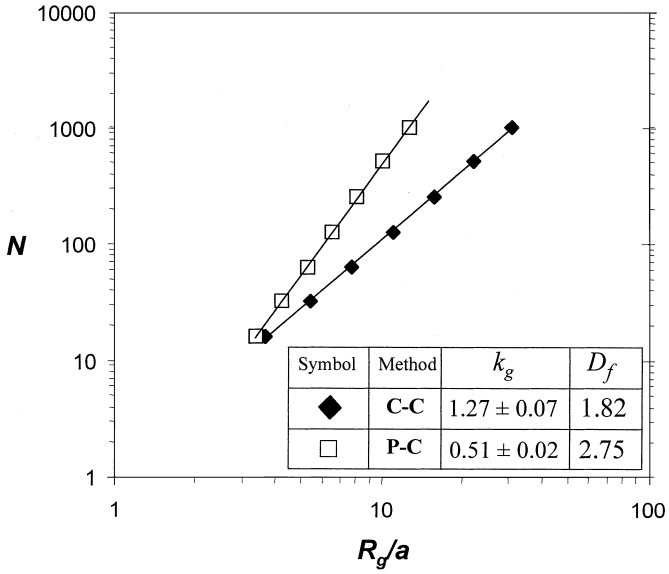

Fig. 4. Number of particles per aggregate versus normalized radius of gyration yielding fractal dimension and fractal pre-factor for cluster–cluster and particle–cluster aggregates.

and are difficult to characterize from projected images, justifying the analysis of this class of aggregates.

3.1.2. Coordination number distribution function

The strength of an aggregate depends on the attractive forces between component particles and the number of P–P contacts. Thus, a physically relevant characterization of aggregated matter is provided by the mean coordination number, Z. Coordination number distribution functions of aggregates identify the number of contacts between primary particles. For example, particles arranged in a straight chain ($D_f = 1.0$) have $Z = 2$, while for aggregates with more compact structures, Z tends to increase. A change in Z generally implies that aggregate properties such as thermal conductivity or fabric tensor will change appreciably.

In Fig. 5, the coordination number distribution functions are presented for C–C and P–C aggregates with different number of primary particles per aggregate. Results obtained indicate that the coordination number distribution function for C–C aggregates is nearly independent of aggregate size. Moreover, for this class of aggregates it peaks at $Z = 2$, indicating that most of the aggregates are composed of clusters of elongated chains. Therefore, it is expected that, for a specific fractal dimension, the coordination number distribution function should be universal, i.e., independent of aggregate size for C–C aggregates.

For P–C aggregates, there is a slight effect of aggregate size on the coordination number distribution function. In particular, the weight of the outer particles — the "membrane" (characterized by $Z = 1$) — tends to decrease as the aggregates become bigger. Therefore, the dominant effect of $Z = 1$ decreases while intermediate values of Z become more important. Additionally, the relative importance of the nucleus of the aggregate becomes less dominant as the aggregate

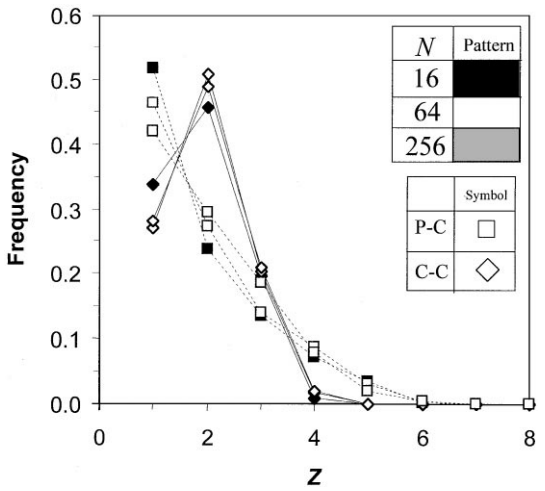

Fig. 5. Coordination number distribution function for simulated cluster–cluster and particle–cluster aggregates with different number of primary particles.

increases while the "cytoplasm" increases. In conclusion, intermediate values of Z appear to become more important as the aggregate becomes bigger. However, for the range of aggregate sizes considered the dominant value appears to be $Z = 1$.

3.1.3. Distribution of angles between triplets

An additional relevant property of aggregated matter is the distribution of angles between triplets (also designated as trimers, Elimelech, Gregory, Jia, & Williams, 1995), defined as the largest angle in the triangle formed by the centers of three touching primary particles. Clearly, for a triplet of equal spheres, the bond angle must be between 60 and 180°; for partially sintered particles with polydisperse sizes this range may be extended. This property can be useful in describing the stability of aggregate morphology, their capacity to condense vapors, and the final shape of an aggregate that undergoes restructuring. In addition, the evolution of the distribution of angles between triplets is important to characterize the change of morphology of aggregates due to the restructuring mechanisms of Brownian motion, surface energy driven viscous flow, and/or capillary condensation (Tassopoulos & Rosner, 1992).

In Fig. 6, histograms of angles between triplets are shown for C–C and P–C aggregates having different number of touching uniform-size primary particles. Although the scatter of results is quite significant, aggregate size appears to have no appreciable effect on this property. The histogram has a peak near 100–120° for C–C aggregates decreasing for larger and lower angles. On the other hand, P–C aggregates exhibit a different trend. Except for small aggregates, the frequency is approximately constant for angles between 60 and 120° and continuously decreases as the angle increases reaching a minimum at 180°. Despite the lack of experimental data published in the literature, C–C results obtained were compared with data reported by Cohen and Rosner (1993) and Elimelech et al. (1995). Experimental histograms presented by these authors have maximum frequencies between 90 and 100°, showing very good agreement with numerical results obtained in the present work.

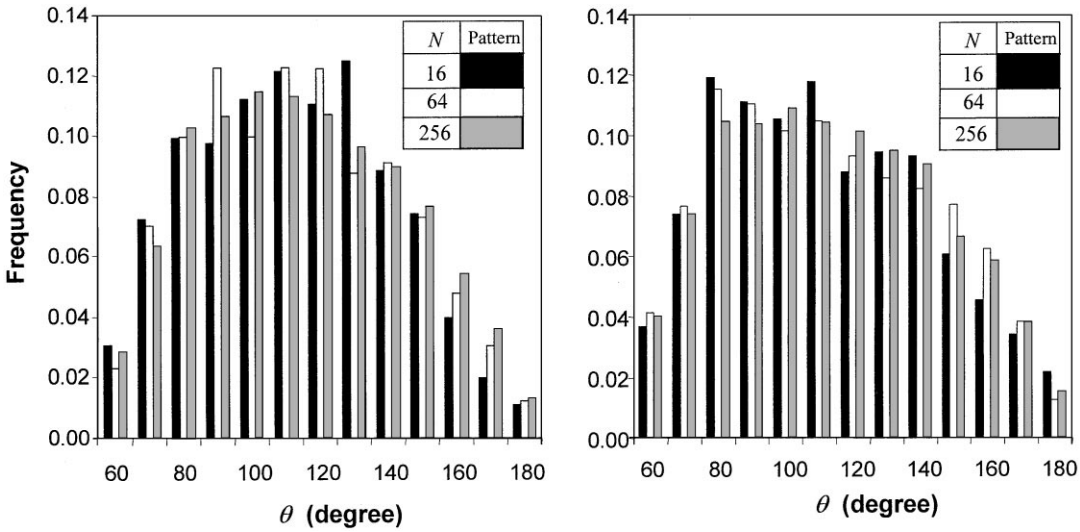

Fig. 6. Histogram of the angle between triplets for simulated cluster–cluster and particle–cluster aggregates with different number of primary particles.

3.2. Effects of partial sintering on the morphological properties of C–C aggregates

Partial sintering of C–C aggregates due to the overlapping of neighboring primary particles is analyzed here for the different morphological properties previously identified, namely the radius of gyration, coordination number distribution function, distribution of angles between triplets, and fractal properties. One issue that needs to be clarified is how one can estimate the penetration coefficient, C_p, in view of the fact that the projection of a three-dimensional aggregate leads to additional overlapping. Based on simulated C–C aggregates, Brasil et al. (1999a) suggested a method to estimate C_p from the projected image of an aggregate. After observing projected images of more than 300 uniform-size spherule couples, they compared the projected penetration coefficients with the actual three-dimensional values that were assigned while constructing the aggregates. Results obtained indicated that the actual penetration coefficient scales with the projected one in the following manner:

$$C_p = \zeta_1 C_{p,proj} - \zeta_2, \quad \text{where } \zeta_1 = 1.1 \pm 0.1 \text{ and } \zeta_2 = 0.2 \pm 0.02. \tag{3}$$

Accordingly, Brasil et al. (1999a) suggested that it should be possible to obtain the actual C_p from TEM images by measuring $C_{p,proj}$ of several primary particle couples — preferably near the tips of projected aggregate images — and using the correlation given in Eq. (3).

3.2.1. Radius of gyration

Partial sintering will unavoidably make the aggregates more compact as viewed in Fig. 2. This is intuitive based on the method adopted to simulate this effect in which centers of primary particles approach each other. The main question is therefore as follows: can the effect of partial sintering on aggregate size be quantified in terms of the penetration coefficient? Fig. 7 shows aggregate radius of

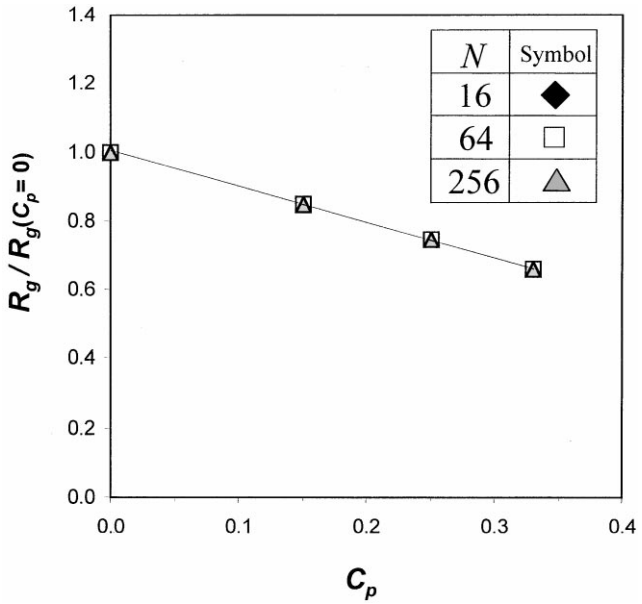

Fig. 7. Variation of the radius of gyration with the penetration coefficient, C_p.

gyration relative to the one with no overlapping ($C_p = 0$) as a function of penetration coefficient for different aggregate sizes. It is interesting to note that the results in Fig. 7 are independent of number of primary particles in aggregates, N. In addition, the effect of partial sintering on the radius of gyration exhibits a linear behavior. Based on these trends, we obtained the following expression (line plotted in Fig. 3) to estimate the radius of gyration of an aggregate with overlapping monomers:

$$R_g/R_g(C_p = 0) = 1 - C_p. \tag{4}$$

3.2.2. Coordination number distribution function

The coordination number, Z, indicates the number of bonds that each particle has and therefore describes (together with C_p) the rigidity of the aggregate. C–C fractal-like aggregates exhibit an open-structure shape formed by elongated branches. Consequently, it is expected that these aggregates have a coordination distribution function peaking at around $Z = 2$. This can be confirmed in Fig. 8 where these functions are plotted for different aggregate sizes with and without considering partial sintering. The results shown point out that the coordination distribution function is relatively insensitive to the aggregate size. This was expected because the larger aggregates were formed from connecting two smaller aggregates during our computer simulations. Moreover, overlapping apparently leads to stronger bonds as indicated by an increase from 2 to 3 in Z when C_p is increased from 0 to 0.25. In summary, the real overlapping that unavoidably occurs in any type of aerosol will contribute to increase the mean coordination number and therefore the compactness and rigidity of the aggregate structure.

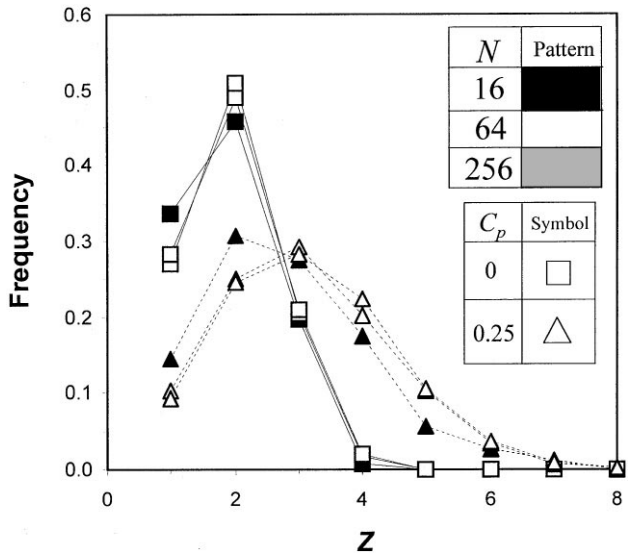

Fig. 8. Coordination number distribution function for simulated cluster–cluster aggregates with different penetration coefficient, C_p.

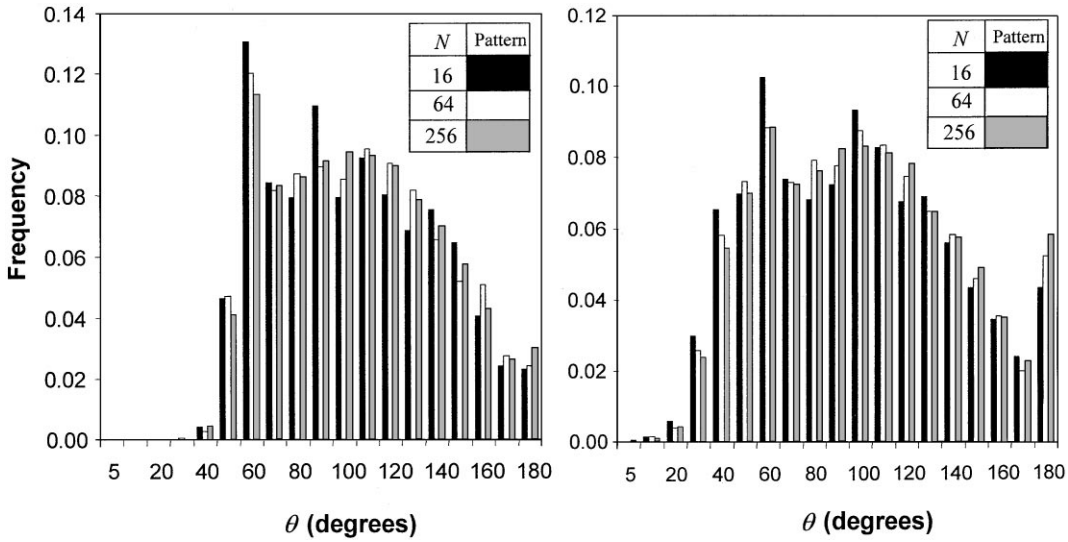

Fig. 9. Histogram of the angle between triplets for simulated cluster–cluster aggregates with different number of primary particles for penetration coefficients of $C_p = 0.15$ and 0.25.

3.2.3. Distribution of angles between triplets

Fig. 9 includes a histogram of the angle between triplets for C–C aggregates with different partial sintering rates. When the results of C–C aggregates shown in Fig. 6 are compared with the ones in Fig. 9, it is observed that an increase in partial sintering shifts the higher frequencies to smaller

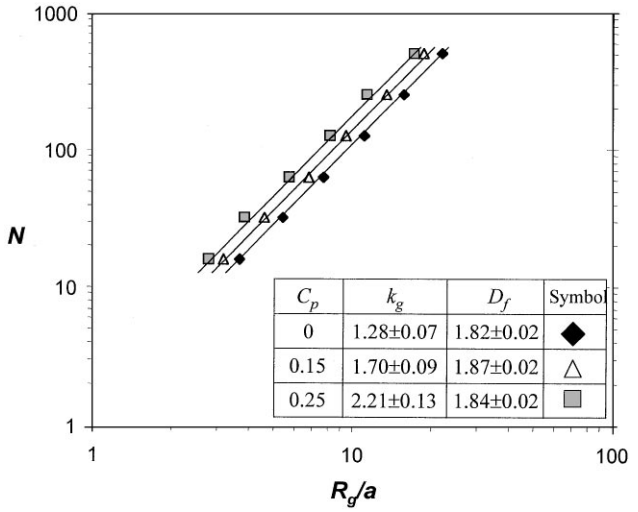

Fig. 10. Number of primary particles per aggregate versus normalized radius of gyration for simulated aggregates with different penetration coefficients.

angles. Yet, angles for just-touching particles are not less than 60°, while higher frequency of angles smaller than 60° can also be found with an increase in the penetration coefficient.

3.2.4. Fractal properties

The morphology exhibited by C–C aggregates is quite complex, as shown in Figs. 1 and 2. Fractal theories have tried to unify most of the structural characteristics, namely the fractal dimension, D_f, and, more recently, the fractal pre-factor, k_g. Knowledge of these properties is a key issue in fully characterizing fractal-like aggregates. The fractal dimensions of aggregates suffering partial sintering are illustrated in Fig. 10, in which the number of primary particles in aggregates, N, is plotted against the relative radius of gyration, R_g/a. While D_f represents the slope, k_g describes where the least-squares linear fit intersects the vertical axis in a logarithmic plot N versus R_g/a. Results obtained are fairly conclusive, in particular: (i) aggregates constructed with and without partial sintering act like mass fractals; (ii) the fractal dimension, D_f, appears to be insensitive to partial sintering; (iii) the fractal pre-factor is strongly affected by partial sintering. Based on the results obtained, we suggest the following expression to estimate the variation of k_g with the penetration coefficient, C_p:

$$k_g = 1.3 \exp(2.2 C_p). \tag{5}$$

The fact that partial sintering leads to an increase in the fractal pre-factor is an important conclusion that is capable of justifying the systematic gap between the numerical and experimental fractal properties published by various investigators. Although the fractal dimension of C–C aggregates appears to be an established property (1.6–1.9), the existence of a universal value for the fractal pre-factor is still a controversial issue. Wu and Friedlander (1993) and, more recently, Koylu et al. (1995b) have unified most of the numerical and experimental data reported on this property. For example, for C–C aggregates, results published in the literature for k_g range from 1.23

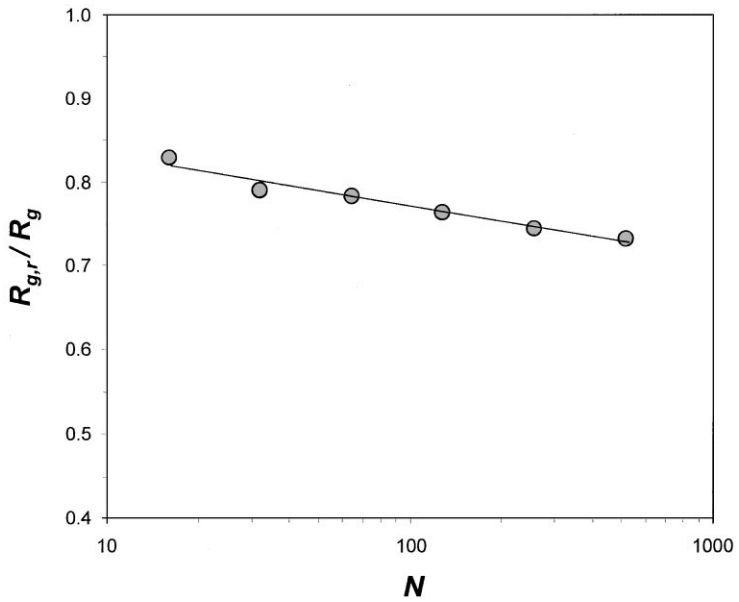

Fig. 11. Influence of the restructuring process on the radius of gyration of simulated cluster–cluster aggregates.

(Cai et al., 1995) to 3.47 (Samson et al., 1987). If we take into account that penetration parameter, C_p, varies from 0 to 0.3, Eq. (5) yields k_g between 1.3 and 2.5. These values without and with partial overlapping of primary particles fall well within the limits of the previous studies mentioned above. Thus, k_g values based on numerically simulated aggregates are generally smaller than the ones inferred from experimental data, simply because of not accounting for overlapping of spherules. Note that this interpretation for the effect of partial sintering on k_g is totally different from that of Oh and Sorensen (1997), who concluded that particle overlapping could not be responsible for the difference between simulations and experiments.

3.3. Effects of restructuring on the morphological properties of C–C aggregates

As previously presented, restructuring is numerically simulated assuming that the rigidity of the contact point between two clusters may not be sufficient, and, therefore, an additional bond is required. If this is a constant pattern in most fractal-like aggregates, it clearly depends on the fractal nature as well as the environment where particles are generated. However, it is expected to occur at least partially throughout the complex processes involved in particle production. The following sub-sections will focus on the limiting case where all steps involving the bond of two clusters will also include a restructuring procedure.

3.3.1. Radius of gyration

Because restructuring leads to more compact aggregates, a reduction of the radius of gyration is indeed expected. This trend can be confirmed in Fig. 11 where the effect of restructuring on the radius of gyration is plotted against aggregate size, N. Results suggest that R_g reduction increases

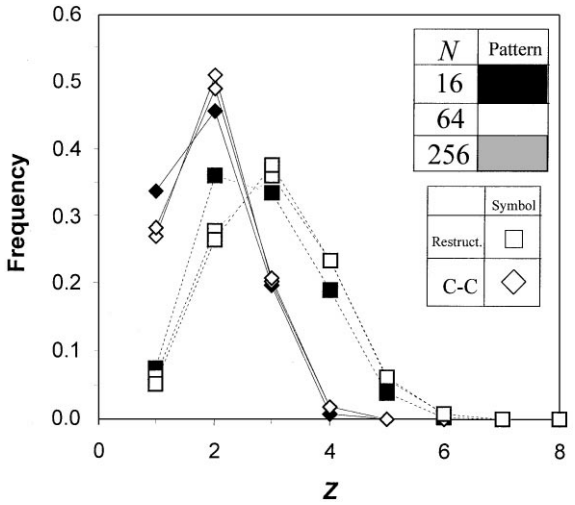

Fig. 12. Influence of the restructuring process on the coordination number distribution function for simulated cluster–cluster aggregates with different number of primary particles.

moderately with aggregate size in an exponential way with the least-squares fit yielding

$$R_{g,r}/R_g = 0.9N^{-0.034}. \tag{6}$$

3.3.2. Coordination number distribution function

Restructuring acts as a natural way of increasing the number of bonds between neighboring primary particles. In fact, the physical nature of restructuring is directly related to increasing the rigidity of the aggregate by having more contact points between clusters that attach to each other. Therefore, results obtained for the coordination distribution function shown in Fig. 12 are a logical corollary of the latter. The mean value of Z suffers a similar shift as seen previously when investigating the effects of partial sintering. Once again, aggregate size appears to play no dominant role in this situation.

3.3.3. Distribution of angles between triplets

As previously seen, the restructuring mechanism involves a shift of the mean coordination number from 2 to 3. Consequently, it was expected that the angle between triplets most frequently found should be about 60°. This can be confirmed in Fig. 13 where histograms of angles between triplets are plotted for aggregates with restructuring and compared with the standard situation.

3.3.4. Fractal properties

As a result of restructuring, aggregates will unavoidably exhibit a more compact structure. This can be confirmed through the results shown previously in Figs. 11 and 12 where R_g decreases and Z increases with restructuring. While the fractal dimension can be used as a measure of the openness of the structure of an aggregate (i.e., how far apart the branches are from each other), the fractal pre-factor, k_g, is more related to the void that exists between the primary particles. This

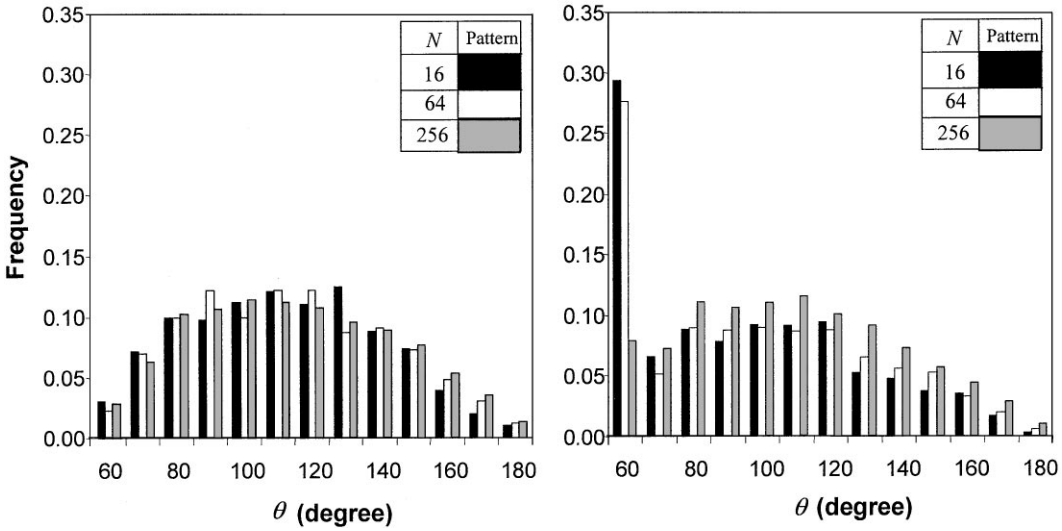

Fig. 13. Histogram of the angle between triplets for simulated cluster–cluster aggregates with different number of primary particles: (a) without restructuring; and (b) with restructuring.

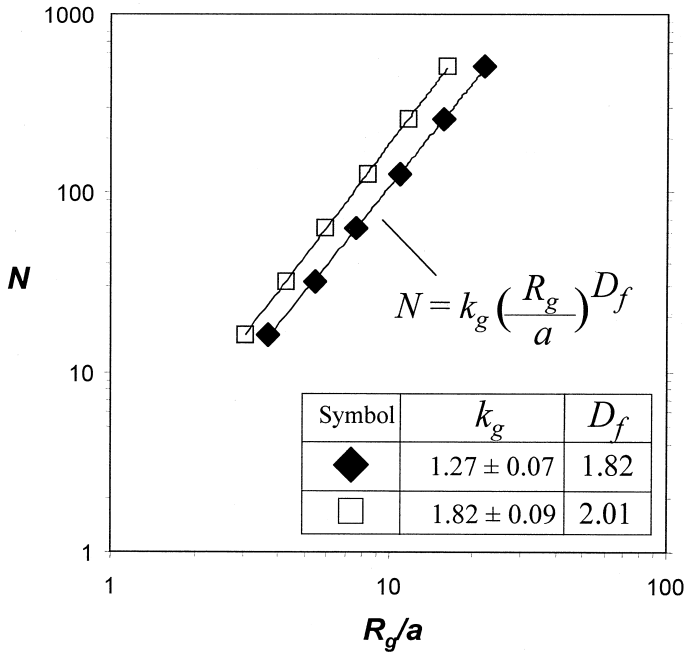

Fig. 14. Influence of the restructuring process on the fractal properties of cluster–cluster aggregates.

simple way of interpreting the two basic fractal properties will be useful in analyzing the results shown in Fig. 14 where N is plotted against R_g/a, showing the effect of restructuring on D_f and k_g. Predictions shown in Fig. 14 indicate that both fractal properties suffer slight increases due to the

restructuring model. Specifically, the fractal dimension approaches 2, an upper value of typical C–C aggregates, indicating that partial restructuring may occur in real aggregates. Although the fractal pre-factor also increases roughly by 25%, this increase is quite small when compared to the variation of k_g with partial sintering that can go above 100%.

4. Summary and conclusions

In the present study, morphologies of both C–C and P–C fractal-like aggregates were investigated. Statistically significant populations of numerically simulated aggregates were generated in order to characterize three-dimensional morphological properties of aggregates, including fractal dimension, fractal pre-factor, coordination number distribution function, and distribution of angles between triplets. Effects of C–C and P–C aggregation mechanisms and aggregate size were also taken into consideration. Moreover, the morphological properties of aggregates undergoing partial sintering and restructuring were investigated. The population studied was composed of ca. 450 simulated aggregates having the number of primary particles per aggregate, N, between 8 and 1024. The main conclusions of the present study can be summarized as follows:

1. Coordination number distribution functions of C–C aggregates appear to be independent of aggregate size having a maximum value at $Z = 2$. On the contrary, for P–C aggregates this function shows that the dominant value equals 1. Coordination number distribution function is similarly affected by restructuring and partial sintering. Both effects lead to an increase in the mean value. While larger R_g indicates that aggregates are more compact, larger Z implies stronger structure with more bonds per volume.
2. Distributions of angle between triplets are fairly independent of aggregate size. However, the formation mechanism is a relevant parameter, that is, the dominant angles for C–C aggregates fall between 100 and 120° whereas P–C aggregates tend to exhibit smaller angles. Restructuring simply shifts the most probable angle to 60°.
3. Partial sintering of particles strongly reduces the radius of gyration of an aggregate. This effect appears to be independent of aggregate size and can be estimated using the following relation: $R_g/R_g(C_p = 0) = 1 - C_p$. Although less affected by restructuring, the magnitude of the reduction of the radius of gyration also increases with aggregate size as follows: $R_{g,r}/R_g = 0.9N^{-0.034}$.
4. While partial sintering leads to virtually no variation in the fractal dimension, restructuring slightly increases D_f to ca. 2.0. More importantly, the fractal pre-factor is strongly affected by partial sintering. Based on the results obtained, the following expression to estimate the variation of k_g with the penetration coefficient, C_p, is suggested: $k_g = 1.3\exp(2.2C_p)$. This may justify the systematic gap between the numerical and experimental results reported by different investigators for k_g.

Acknowledgements

A. M. Brasil would like to acknowledge the scholarship of Conselho Nacional de Desenvolvimento Científico e Tecnológico — CNPq. U. O. Koylu was sponsored by the U.S. National Science Foundation (Grant Nos. CTS-9711954 and CTS-9876475).

References

Botet, R., & Jullien, R. (1988). A theory of aggregating systems of particles: The clustering of clusters process. *Annales Physics Francias*, *13*, 153.

Brasil, A. M., Farias, T. L., & Carvalho, M. G. (1999). A recipe for image characterization of fractal-like aggregates. *Journal of Aerosol Science*, *33*, 1379–1389.

Brasil, A. M., Farias, T. L., & Carvalho, M. G. (2000). Evaluation of the fractal properties of cluster–cluster aggregates. *Aerosol Science and Technology*, in press.

Cai, J., Lu, N., & Sorensen, C. M. (1995). Analysis of fractal cluster morphology parameters: Structural coefficient and density autocorrelation function cutoff. *Journal of Colloid Inteface Science*, *171*, 470–473.

Cohen, R. D., & Rosner, D. E. (1993). *Kinetics of restructuring of large multi-particle aggregates*. AAAR Paper No. 8D4.

Eden, M. (1961). A two-dimensional growth process. In J. Newman (Ed.), *Fourth Berkeley symposium on mathematics, statistics and probability*, vol. IV: *Biology and the problems of health* (pp. 223–239). Berkeley: University of California Press.

Elimelech, M., Gregory, J., Jia, X., & Williams, R. (1995). *Particle deposition & aggregation*. Oxford: Butterworth-Heinemann.

Farias, T. L., Carvalho, M. G., & Koylu, U. O. (1996). Range of validity of the Rayleigh–Debye–Gans theory for optics of fractal aggregates. *Applied Optics*, *35*, 6560–6567.

Farias, T. L., Carvalho, M. G., Koylu, U. O., & Faeth, G. M. (1995). Computational evaluation of approximate Rayleigh–Debye–Gans/fractal-aggregate theory for the absorption and scattering properties of soot. *Journal of Heat Transfer*, *117*, 152–159.

Gouyet, J. -F. (1996). *Physics and fractal structures*. New York: Springer.

Hutchinson, H. P., & Sutherland, D. N. (1965). An open-structured random solid. *Nature*, *206*, 1036–1037.

Jullien, R., & Botet, R. (1987). *Aggregation and fractal aggregates*. Singapore: World Scientific.

Koylu, U. O., Faeth, G. M., Farias, T. L., & Carvalho, M. G. (1995a). Fractal and projected structure properties of soot aggregates. *Combustion and Flame*, *100*, 621–633.

Koylu, U. O., Xing, Y., & Rosner, D. E. (1995b). Fractal morphology analysis of combustion-generated aggregates using angular light scattering and electron microscope images. *Langmuir*, *11*, 4848–4854.

Meakin, P. (1983a). Diffusion-controlled cluster formation in two, three and four dimensions. *Physics Review A*, *27*, 604–607.

Meakin, P. (1983b). Diffusion-controlled cluster formation in 2–6 dimensional space. *Physics Review A*, *27*, 1495–1507.

Meakin, P. (1984). Computer simulation of cluster–cluster aggregation using linear trajectories: Results from three-dimensional simulations and comparison with aggregates formed using brownian trajectories. *Journal of Colloid Interface Science*, *102*, 505–512.

Megaridis, C. M., & Dobbins, R. A. (1990). Morphological description of flame-generated materials. *Combustion Science and Technology*, *71*, 95–109.

Mountain, R. D., & Mulholland, G. W. (1988). Light scattering from simulated smoke agglomerates. *Langmuir*, *4*, 1321–1326.

Nelson, J. A., Crookes, R. J., & Simons, S. (1990). On obtaining the fractal dimension of a 3D cluster from its projection on a plane — application to smoke agglomerates. *Journal Physics D: Applied Physics*, *23*, 465–468.

Oh, C., & Sorensen, C. M. (1997). The effect of overlap between monomers on the determination of fractal cluster morphology. *Journal of Colloid Interface Science*, *193*, 17–25.

Samson, R. J., Mulholand, G. W., & Gentry, J. W. (1987). Structural analysis of soot agglomerates. *Langmuir*, *3*, 272–281.

Sorensen, C. M., & Feke, G. D. (1996). The morphology of macroscopic soot. *Aerosol Science and Technology*, *25*, 328–337.

Sorensen, C. M., & Roberts, G. C. (1997). The prefactor of fractal aggregates. *Journal of Colloid Interface Science, 186*, 447–454.

Sutherland, D. N. (1967). A theoretical model of floc Structure. *Journal of Colloid Interface Science, 25*, 373–380.

Tassopoulos, M., & Rosner, D. E. (1992). Microstructural descriptors characterizing granular deposits. *A.I.Ch.E.* Journal, *38*, 15–25.

Vold, M. J. (1963). Computer simulation of floc formation in a colloidal suspension. *Journal of Colloid Science*, *18*, 684–695.

Witten, T. A., & Sander, L. M. (1981). Diffusion-limited aggregation, a kinetic critical phenomenon. *Physics Review Letters*, *47*, 1400–1403.

Witten, T. A., & Sander, L. M. (1983). Diffusion-limited aggregation. *Physics Review B*, *27*, 5685–5697.

Wu, M., & Friedlander, S. K. (1993). Note on the power-law equation for fractal-like aerosol agglomerates. *Journal of Colloid and Interface Science*, *159*, 246–248.